Microfluidic platform for environmental contaminants sensing and degradation based on boron-doped diamond electrodes

Mariana Medina-Sánchez[1,+], Carmen C. Mayorga-Martinez[1,+], Takeshi Watanabe[2], Tribidasari A. Ivandini[2,3], Yuki Honda[2], Flavio Pino[1], Yasuaki Einaga[2,4] and Arben Merkoçi[1, 5*]

[1]Nanobioelectronics & Biosensors Group. Institut Catala de Nanociencia I Nanotecnologia (ICN2).

[2] Department of Chemistry, Keio University, 3-14-1 Hiyhoshi-Yokohama, 223-5822, Japan.

[3] Department of Chemistry, Faculty of Mathematics and Sciences, University of Indonesia, Kampus UI Depok, Jakarta 16424, Indonesia.

[4] JST-CREST, 3-14-1 Hiyoshi, Yokohama 223-5822.

[5] ICREA, Institució Catalana de Recerca I Estudis Avançats.

[+] These authors contributed equally to this work.

* Email: arben.merkoci@icn.cat , Tel: +34937374604.

Abstract. We have developed a lab-on-a-chip (LOC) platform for electrochemical detection and degradation of the pesticide atrazine (Atz). It is based on boron-doped diamond (BDD) electrodes and a competitive magneto-enzyme immunoassay (EIA) that enables high sensitivity. To detect the enzymatic reaction, we employed a BDD electrode modified with platinum nanoparticles (PtNPs), as a highly conductive catalytic transducer. Chronoamperometry revealed a limit of detection (LOD) of 3.5 pM for atrazine, which, to the best of our knowledge, is one of the lowest value published to date. Finally, we degraded Atz in the same platform, using a bare BDD electrode that features remarkable corrosion stability, a wide potential window, and much higher O_2 overvoltage as compared to conventional electrodes. These characteristics enable the electrode to produce a greater amount of $HO^{\bullet}$ on the anode surface

than do conventional electrodes and consequently, to destroy the pollutant more rapidly. Our new LOC platform might prove interesting as a smart system for detection and remediation of diverse pesticides and other contaminants.

Keywords: Boron-doped diamond electrodes, electrochemistry, microfluidics, pesticide detection, and pesticide degradation.

1. Introduction

Destruction of pesticides such as atrazine is crucial for minimizing their damage to human health and to the environment. Atrazine and its degradation products are triazine herbicides, which are the most commonly found toxic agents in groundwater. Moreover, due to its polarity, atrazine is a persistent environmental contaminant. This herbicide is extensively used for selective control of annual grasses and broad-leaved weeds **(Hernandez et al., 1998; Leovac et al., 2015)** but has mutagenic effects on the reproductive system **(George et al., 1995)**. Thus, there is a pressing need for methods and tools to detect and destroy atrazine from waste, ground and tap waters *in situ*.

Albeit several methods for pesticide detection have been reported, most of them require sample pre-treatment, purification procedures, large reagent-volumes, expensive equipment and trained personnel. Furthermore, the conventional methodologies are expensive and time-consuming. Therefore, the development of portable, low-volume and easy-to-use quantification devices is of great interest. Microfluidics systems are an especially attractive option, due to their amenability to miniaturization, low volume requirements, facile transducer integration and low cost **(Drechsel et al., 2015)**.

Immunosensing technologies—particularly, those based on labeling strategies—have garnered interest for pesticide detection, owing to their high specificity and sensitivity. The integration of

immunoassays with microfluidic platforms is an appealing option to obtain devices that are simpler, faster and more sensitive than are classical tools **(Maleki et al., 2007)**.

In recently developed sensors and biosensors, nanomaterials have proven extremely utile for transducer modification, enabling enhanced measurements based on electrochemical (amperometric, impedimetric, potentiometric), optical (light absorbance, dispersion, fluorescence) or mixed signals (*e.g.* electrochemiluminescence and nanomechanics) **(Merkoçi et al., 2010; Aragay et al., 2011, 2012)**. Of special interest is the application of nanomaterials in lab-on-a-chip (LOC) systems **(Merkoçi et al., 2012; Medina-Sánchez et al., 2012)** including the use of magnetic beads for capture/pre-concentration to improve enzymatic **(Llopis et al., 2009)** or immunological **(Ambrosi et al., 2011)** reactions, an advantage that stems from their high surface area, fast assay kinetics and ready manipulation.

Different strategies have been proposed for removal and degradation of pesticides from waste, ground and tap waters, including photo-catalysis **(Affam et al., 2013; Malpass et al., 2010)** Fenton-like catalysis **(Oturan et al., 2010)** and anodic oxidation **(Samet et al., 2010)**. Among these strategies, anodic oxidation is an emergent method for the direct destruction of organic pollutants **(Vera et al., 2009; Borràs et al., 2010).** This electrochemical process is based on two steps: oxidation of water to form hydroxyl radicals ($HO^{\bullet}$) at the anode surface (see Eq. 1), and subsequent reaction of the radicals with the target pesticides.

$$H_2O \rightarrow HO^{\bullet} + H^+ + e^- \qquad \text{(Eq. 1)}$$

We integrated a boron-doped diamond (BDD) electrode into an LOC platform to obtain a platform that can efficiently detect and degrade the pesticide atrazine via electrochemical reactions. For detection, we used a BDD electrode modified with platinum nanoparticles (PtNPs). We chose BDD electrodes because they exhibit low adsorption of organic contaminants—a quality that, when used in flow systems, provides a clean surface that ensures repeatability **(Min-Jung et al., 2011)**. Moreover,

BDD electrodes offer high electrical conductivity and low background current, which enable excellent signal-to-noise ratios in applications such as ours. Additionally, PtNPs offer interesting catalytic properties for enzymatic reactions **(Fierro et al., 2012; Zou et al., 2008)**. We combined the various properties of this BDD electrode with the benefits of on-chip magnetic-bead manipulation.

For degradation of atrazine, we used three electrodes-system where an unmodified BDD electrode is used as anode, a carbon electrode as cathode and Ag/AgCl as reference electrode. BDD is the most promising material for electrochemical application due to its inert nature, remarkable stability to corrosion, and extremely wide potential-window in aqueous media. Moreover, BDD anodes offer much higher O_2 overvoltage than do conventional anodes (*e.g.* carbon, platinum or gold ones), thereby producing a greater amount of $HO^{\bullet}$ onto its surface **(Marselli et al., 2003)** and consequently, enabling more rapid destruction of pollutants **(Samet et al., 2010)**. Furthermore, our new strategy for pollutant destruction is environmentally friendly, as it does not generate any toxic waste.

Scheme 1 is a schematic of our platform for atrazine detection and degradation (for photographs of the actual platform, see Figure S1, in the Supporting Information). The platform is based on a hybrid polydimethylsiloxane-polyester (PDMS-PE) chip with the two integrated BDD electrodes (described above). Early results with this type of platform suggested that it might be an excellent general device for detecting and destroying pollutants such as pesticides.

Scheme 1

2. Experimental

2.1. Reagents

The atrazine magneto-ELISA kit was purchased from Abraxis (Pennsylvania, USA). For the atrazine derivatization, the following reagents were used (all purchased from WAKO, Japan): standard atrazine ((2-

chloro-4-(ethylamino)-6-isopropylamino-s-triazine), 3-mercaptopropanoic acid, KOH, absolute ethanol, sodium bicarbonate ($NaHCO_3$) and chloroform. Potassium tetrachloroplatinate (K_2PtCl_4), phosphate buffered saline (PBS) and 3-aminopropyltriethoxylane (APTES) were purchased from Sigma-Aldrich, Spain. The screen-printed inks (graphite ink [Electrodag 423SS] and Ag/AgCl ink [Electrodag 6037SS]) were purchased from Acheson Industries, USA. Diamond powder and negative photoresist were purchased from Kemet corp., UK; and SU-8, from Microchem (Newton, MA, USA).

2.2. Instruments

Electrochemical measurements were performed with an Autolab (Echo Chemie, The Netherlands), two syringe pumps (standard infusion only; model: Pump 11 Elite; Harvard Apparatus [USA]) were used for separately injecting the conjugated stock solution and the buffer PBS. Scanning electron microscopy (SEM) analysis was performed on a FEI MAGELLAN 400L SEM High resolution microscope (USA). Raman spectroscopy (Renishaw System 2000, UK) was used for evaluating the BDD film formation. Home-made electrodes (SPCEs) were fabricated by screen-printing technology using a screen-printer (DEK 248, UK). Polycrystalline BDD thin films were grown on Si (111) substrates using a 2.45 GHz microwave plasma chemical vapor deposition (CVD) system equipped with a 6 kW microwave plasma CVD reactor (Model AX6500 CORNES Technologies Corp., Japan).

2.3. Preparation of BDD electrodes

The BDD films were prepared as reported elsewhere **(Einaga, 2010; Suzuki et al., 2007)**. To enhance the diamond nucleation density, the silicon substrates were pre-treated by abrasion with diamond powder (diameter: *ca.* 1 μm), and subsequently cleaned by ultra-sonication in distilled water and isopropyl alcohol. The film was grown at a pressure of 80 torr with a total gas flow of 500 sccm. A

hydrogen/methane/trimethylboron gas mixture was used, with a methane/hydrogen ratio of 4:96 and a carbon/boron ratio of 1:99. A deposition time of 4 h was used, which gave a film thickness of *ca.* 2 μm.

2.4. Fabrication of microfluidic channel and integration of BDD electrodes

The microfluidic platforms were fabricated by rapid prototyping and PDMS technologies, as previously described **(Xia et al., 1998)**. Briefly, a 4-inch silicon wafer was spin-coated with a negative photoresist and patterned by photolithography by using a flexible mask. PDMS was poured onto the resulting mold and cured at 65 ºC for 2 h. The channels were 3.5 mm wide, 100 μm deep and 1 cm long. Two reservoirs were punched: one at the channel inlet, and one at the channel outlet. The electrochemical cell for detection and degradation comprised a set of three electrodes: a *counter electrode* (graphite); a *reference electrode* (Ag/AgCl) fabricated by screen-printing technology using a screen printer (DEK 248); and a previously fabricated BDD *working electrode* (WE). Screen-printed electrodes are based on the sequential deposition of graphite ink and Ag/AgCl ink. After deposition, each layer was dried. Finally, the polyester sheet substrate was maintained at 120 ºC for 45 min (graphite) and 30 min (Ag/AgCl). Next, the PDMS channel and polyester sheet (PE) substrate were assembled using a literature protocol **(Tang et al., 2010)**. The polyester substrate was treated by air-plasma for 1 min, and then immersed into a 2% (v/v) aqueous solution of APTES for 1 h in order to activate the surface. The surface of the PDMS channel was also activated for 1 min by plasma, and then placed into contact with the PE sheet to achieve irreversible bonding. Once the first bonding had terminated, the BDD wafer was integrated as working electrode, by attachment using double-sided adhesive tape. Previously, a 3-mm hole had been drilled in the PE, in between the counter and reference electrodes.

Two different channels were fabricated: a simple channel (width 3 mm; height 200 μm; and length: *ca.* 20 mm) used for detection and degradation; and a micro-mixer used for the immunoassay (cross-section: width 500 μm; height 100 μm; and length: 480 mm). The micro-mixer dimensions were optimized to obtain

the optimal geometry for ensuring the mixing with the different biomolecules, which is also related to the conjugation efficiency (not shown result).

2.5. Formation of platinum particles

In the detection module, platinum particles (PtNPs) were grown by electrodeposition of a solution of K_2PtCl_4 (25 mM) in phosphate buffer (pH 7.2) through application of -0.75 V for 100 s onto the BDD working electrode (which had previously been integrated into the microfluidic channel). This potential value corresponds to the platinum reduction peak on BDD working electrode, as previously determined using cyclic voltammetry. The electrodeposition was done in static mode.

2.6. Derivatization of atrazine

A carboxylic acid derivative of atrazine (Atz), 3-{4-(ethylamino)-6-[(1-methylethyl)amino]-1, 3,5-triazin-2-yl} propanoic acid, required for conjugation of atrazine to HRP, was synthesized as described by Smyth *et al*. **(Grennan et al., 2003)**. Briefly, a solution of 5.4 mmol 3-mercaptopropanoic acid, 10.8 mmol 85% (w/v) KOH and 10 mL absolute ethanol was added to a stirred homogeneous mixture of 5 mmol atrazine and 100 mL absolute ethanol. The mixture was refluxed under nitrogen for 5 h until a white solid remained, which was taken up in 25 mL of 5% (w/v) $NaHCO_3$. This solution was washed with 3 × 10 mL chloroform and acidified to pH 2 with 6 M HCl. The white solid was collected, washed with milli-Q water and dried. Additional product was obtained through evaporation and crystallization of the residue from methanol.

2.7. Optimization of the biosensor variables

To evaluate the performance of the BDD/PtNPs electrode in the HRP response in the presence of H_2O_2, cyclic voltammograms (CVs) were measured at the potential range of -1 to 1 V vs. Ag/AgCl. Amperometric detection was performed by applying -250 mV DC potential vs. Ag/AgCl in 0.1 M phosphate buffer (PBS)

at pH 7.2 with 0.1 M KCl. The measurement time for three conjugated injections was 50 s. All electrochemical experiments were performed at room temperature.

2.8. Magneto-EIA for batch detection of atrazine

An atrazine kit that employs an enzyme-linked immunosorbent assay (ELISA) for determination of atrazine and related triazines was used. Briefly, 200 µL of a solution of derivatized atrazine (at different concentrations), or of the control sample (PBST), were introduced into separate Eppendorf tubes, followed by 200 µL of the atrazine-HRP conjugate, and finally, 400 µL of the magnetic beads functionalized with anti-atrazine antibodies. The mixture was incubated for 30 min at room temperature. The resulting conjugates were then washed three times with PBST, using a magnetic separator, and finally, suspended in 300 µL PBS.

For the colorimetric measurements, a solution of 3,3',5,5'-tetramethylbenzidine (TMB) was added to each Eppendorf tube (300 µL), and the mixture was incubated for 20 min at room temperature. Finally, 300 µL of sulphuric acid (as stopping solution) was introduced into each tube, which caused the TMB to change from blue to yellow. The variation in colour intensity depends on the atrazine concentration, such that a spectrophotometer can be used to quantify the atrazine (λ = 450 nm) within 15 min of adding the stopping solution. The concentration of atrazine is calculated according to a standard calibration curve (*i.e.* concentration of atrazine vs. absorbance at 450 nm).

2.9. On-chip magneto-EIA immunoassay for atrazine detection

Two different on-chip atrazine-detection experiments were performed. The first one was performed for electrochemical measurements in a flow system. Hydrogen peroxide (8 mM) was added to each Eppendorf tube (300 µL) and incubated for 20 min at room temperature. After the incubation, the sample (5 µL) was

introduced into the microfluidic channel, followed by the buffer solution (PBS), and the mixture was measured by amperometry at -250 mV DC (previously optimized potential value).

In the second experiment, the conjugation and the detection were performed in the chip (the mixer chip was used before the detection one). First, the magnetic beads (MB-αAtz, pre-functionalized with anti-atrazine antibodies) were introduced into an Eppendorf tube (600 µL), and then separated with a magnetic separator in order to pre-concentrate them twice (by suspension in 300 µL of PBS). Then, 150 µL of free atrazine in PBS (at 0.09 nM, 0.9 nM, 2.25 nM or 4.5 nM) and 150 µL of atrazine-HRP were mixed together in a separate Eppendorf tube. The next step was to introduce these two solutions (MB-αAtz and free Atz/Atz-HRP), in each mixer inlet and incubate them for 20 min (flow rate: 5 µL/min). Before the incubation, the mixer was connected to the detection microchannel based on the BDD/PtNPs electrodes, using a magnet located behind the working electrode. The conjugate was thereby trapped onto the working electrode. After the incubation step, the mixer was isolated from the detection chip, and the detection chip was washed with washing buffer in order to remove the excess sample (flow rate: 50 µL/min). Finally, 5-µL aliquots of H_2O_2 (8 mM in PBS) were consecutively introduced by using two syringe pumps.

2.10. Electrochemical magneto-EIA for detection of atrazine in spiked samples

Commercial orange juice was diluted five times with Milli-Q water and the pH of the resulting solution was adjusted to 7.2 with sodium hydroxide (in order to match the pH of the PBS used for the immunoreaction). The sample was then filtered through a 0.2 Whatman filter. The atrazine was detected in chip mode, either electrochemically or colorimetrically, as explained above.

2.11. Degradation of atrazine and subsequent detection of residual atrazine

For degradation of atrazine via anodic oxidation, a microfluidic chip (degradation chip) with an integrated bare BDD electrode was added. The outlet of the degradation chip was placed in one of the mixers inlets,

in order to perform the magneto-immunoassay for subsequent detection of residual atrazine (Figure S1B). To find the best conditions for total degradation of atrazine, the applied current was evaluated at 0, 2, 3 and 4 mA. All the degradation experiments were run using a flow rate of 5 µL/min.

3. Results and discussion

3.1. Morphological characterization of the BDD electrodes

We morphologically characterized the two BDD electrodes (bare and PtNP-modified) using scanning electron microscopy (SEM). Figure 1A shows a typical SEM image of a polycrystalline BDD electrode. In the SEM images, homogeneous and well-dispersed PtNPs were observed at the BDD surface (Figure 1B). Moreover, the PtNPs were regularly distributed on the surface. We also confirmed the structure of the BDD films by Raman spectroscopy (Figure 1C), for which we obtained typical spectra that confirmed the sp2 species (single peak at *ca.* 1500 cm^{-1} to 1600 cm^{-1}) and the boron doping (two peaks, at *ca.* 500 cm^{-1} and *ca.* 1200 cm^{-1}) **(Yuan et al., 2012)**. Interestingly, the PtNPs at the surface presented a uniform average diameter of *ca.* 800 ± 10 nm (Figure 1D).

Figure 1

3.2. Optimization of the biosensor for atrazine detection

In the biosensor for atrazine detection, we employed a magneto-enzyme immunoassay (EIA) based on competitive binding between free atrazine and horseradish peroxidase-labeled atrazine (atrazine-HRP) for a limited number of (anti-atrazine) antibodies that were immobilized onto magnetic beads (MBs). Following the protocol explained in the Experimental Section (Figure S2), the MBs functionalized with the atrazine antibody (MBs-α-atrazine) were incubated with both free atrazine and atrazine-HRP. After the incubation, the excess free atrazine and atrazine-HRP was removed by extensive washing.

The resulting magneto-sandwich was immobilized onto the BDD/PtNPs electrode using a magnet located behind it.

To perform the electrochemical measurement, we treated the electrode dropwise with a solution of hydrogen peroxide (H_2O_2) in PBS (8 mM). Cyclic voltammograms (CVs) were taken in the presence and absence of atrazine (4.5 nM). When the BDD/PtNPs electrode was in the presence of free atrazine, the reduction peak decreased and there was a slight shift to more positive potentials (Figure S3A, SI). CVs of the bare BDD electrode (Figure S3B-a) and the BDD/PtNPs electrode (Figure S3B-c) in the presence of MBs-α-atrazine and atrazine-HRP were evaluated using H_2O_2 in PBS (8 mM). With the bare BDD electrode, no signal was observed, whereas with the BDD/PtNPs electrode, a reduction peak for the MBs conjugated with atrazine-HRP appeared at -250 mV. These observations demonstrated that the PtNPs are essential for the enzymatic biosensor. Additionally, a CV was recorded for the BDD/PtNPs electrode in the presence of H_2O_2 in PBS (8 mM) alone, for which a shift to more-negative potentials, and a decrease in magnitude, were observed. These findings indicated that the reduction of H_2O_2 had not interfered with the biosensor signal (Figure S3B-b, SI).

Finally, we took a simple measurement to confirm the operation potential in flow mode. This was done by injecting mixtures of HRP (at different concentrations) and H_2O_2 (0.5 mM) into the microfluidic platform, and then detecting the resulting signal by voltammetry. Interestingly, as the HRP concentration increased, so did the magnitude of the reduction peak (see Figure S3C, SI).

Based on the above results, we confirmed that generation of the catalytic current had been due chiefly to direct electron transfer from the HRP molecules to the BDD/PtNPs electrode. Indeed, HRP in reduced form (HRP-Red) can be chemically oxidized by H_2O_2. Moreover, we observed reduction of the oxidized HRP (HRP-Ox) at -250 mV. We reasoned that since PtNPs enable efficient electron tunneling, they could facilitate electron transfer between the redox protein and the BDD electrode

surface (see Scheme 1 (C')). In this case, the catalytic current was inversely related to the atrazine concentration.

Before testing detection of atrazine using the microchannels, we performed a batch magneto-immunoassay of atrazine samples in the concentration range of 0.0045 nM to 45 nM, evaluating two different types of detection: *electrochemical* (based on cyclic voltammetry) and *colorimetric* (based on absorbance measurements). For the electrochemical detection, the resultant cyclic voltammograms (CVs) were used to build the calibration curve (Figure S4A, SI), which indicated an LOD for atrazine of 1.9 pM. For the colorimetric methods, the resulting absorbance plots were used to build the calibration curve (Figure S4B, SI). As the atrazine concentration increased, the absorbance decreased (*i.e.* the number of antibody binding sites available to form the atrazine-HRP decreased). For the colorimetric measurements, an LOD of 7.2 pM was obtained.

3.3. Atrazine detection using a microfluidic chip based on a BDD/PtNP electrode

We then tested the magneto-EIA for atrazine detection using a simple and cheap microfluidic platform based on PDMS-PE containing integrated hybrid screen-printed electrodes, including the BDD/PtNP electrode as detection platform, and operating in LOC mode (see Scheme 1C). Details of the set-up are provided in the Experimental Section (SI).

Once we had optimized the parameters, we performed the magneto-EIA for on-line detection of atrazine. On-chip measurements were done at a working potential of -250 mV DC; a flow rate of 50 µL/min; and an injection volume of 5 µL. Well-defined plots of current vs. time were observed at different concentrations of atrazine (range: 0.0045 nM to 45 nM) (Figure 2A). The implemented on-chip atrazine biosensor exhibited high performance in terms of sensitivity and LOD (Table S1, SI). The reproducibility was high: for measurements taken using the same chip the RSD was 5.39% (Figure

2B), and for those taken using different chips (performing the magneto-EIA in each one), the RSD was 10.9% (Figure 2C).

Figure 2

3.4. Complete magneto-EIA for atrazine detection by using a micro-mixer

We designed a micro-mixer to perform the conjugation steps for detection of atrazine in flow mode, which enabled us to reduce sample volume, assay times and equipment requirements (see Scheme 1B). We had previously optimized fabrication of the micro-mixer (Figure S5, SI). After the mixing and incubation steps (for details, see the Supporting Information, Experimental Section), the sample was immobilized onto the working electrode in the detection chip (BDD/PtNPs electrode), where a magnet is placed behind it. After the sample pre-concentration, the buffer and 5 μL of H_2O_2 8 mM were injected.

The complete microfluidic platform showed rapid and sensitive electrocatalytic response to atrazine detection. To evaluate the repeatability of this platform, we performed three measurements using three different chips (Figure 3A). The plot in Figure 3B corresponds to the calibration curve for the microfluidic chip in a linear response range (0.9 nM to 4.5 nM), in which r = 0.98. For this system, the achieved LOD was 3.5 pM and the reproducibility was high (RSD of 4.2%).

Figure 3

3.5. Detection of atrazine in spiked samples using chip mode

To further demonstrate the utility of our microfluidic platform for analysis of real samples, we performed recovery tests, using the colorimetric method, on atrazine solutions of different concentrations (range: 0.045 nM to 2.25 nM) in two different matrices: orange juice and PBS (see Figure S6). Figure S6 shows that the device responded similarly to the two matrices, thereby demonstrating the high performance of the magneto-EIA for atrazine detection. Under the same conditions, we also performed a recovery test using the electrochemical method, on a 2.25 nM solution of atrazine in orange juice. In this case, a micro-mixer was used for the conjugation steps of the magneto-EIA. The recovery value for the colorimetric detection was 99.18%, and for the electrochemical detection, 109.33% (see Table S2).

3.6. Atrazine degradation and detection

When a current is applied to a BDD electrode, hydroxyl radicals are produced. Researchers studying this reaction in the presence of atrazine have previously reported that the radicals degrade atrazine into desethylatrazine, desethyldeisopropylatrazine and cyanuric acid^{0} (see Scheme 1A').

We tested degradation of atrazine, using anodic electrochemical oxidation in chip mode (Scheme 1A). The influence of the current on the oxidation of a 30 nM atrazine solution is shown in Figure 4A. As the current was increased up to 4 mA (> 10V), the degradation increased. The same figure shows the current peaks that correspond to post-degradation detection of residual atrazine in chip mode. Under the optimal conditions (4 mA, pH 7 and room temperature), the degradation percentage was *ca.* 97% and the RSD, 2% (see Figure 4B). The current peaks indicated that the higher the current applied through the BDD anode, the lower the detectable concentration of atrazine—suggesting that this electrochemical method offers major improvements over previously reported techniques for pesticide degradation **(Minghua et al., 2011)**. As OH• radicals have been reported to be generated at potentials higher than 2V (vs. Ag/AgCl) **(Madsen et al., 2014)**, we reasoned that a potential value of *ca.* 10 V

(corresponding to current values of *ca.* 4 mA) would be sufficiently high to achieve the optimal level of $OH^{\bullet}$ radicals for efficient atrazine degradation **(Marrero et al., 2009; Chen et al., 2014)**.

Figure 4

4. Conclusions

We have developed a microfluidic platform for the electrochemical detection and degradation of the pesticide atrazine. It is based on a lab-on-a-chip (LOC) with two integrated boron-doped diamond (BDD) electrodes: one electrode whose surface is covered with platinum nanoparticles (PtNPs), for detection of atrazine via a magneto-enzyme immunoassay (EIA); and one bare electrode, for degradation of atrazine via anodic oxidation. The EIA works by competitive binding between free atrazine and horseradish peroxidase-labeled atrazine (atrazine-HRP) for a limited number of (anti-atrazine) antibodies that are immobilized onto magnetic beads (MBs). The catalytic activity of the PtNPs is exploited to induce direct electron transfer from the HRP molecules to the modified electrode. In this work, we have reported the first-ever observation that such a BDD/PtNP system exhibits greater efficiency in a microfluidic platform than in batch experiments. The detection is completely automated and employs a micro-mixer coupled to the BDD/PtNP-based detection platform. Our microfluidic platform showed clear advantages in comparison to other measuring formats such as in-drop or batch, which require sample volumes that are at least one order of magnitude larger and are less sensitive. This microfluidic platform is easy to fabricate, disposable and is amenable to mass production. Very sensitive amperometric detection enabled detection of atrazine at the very low limit of detection (LOD)

of 3.5 pM, which is lower than the maximum contaminant level (130 pM) allowed by the United States Environmental Protection Agency (EPA).

Our microfluidic platform uses a very low DC potential and thus, minimizes possible matrix interference, as we demonstrated through detection of atrazine in orange juice. Moreover, the magneto-EIA assures specific detection. Our platform exhibits a lower LOD than do other systems reported for atrazine detection, such as those based on enzyme-linked immunospecific assay (ELISA). We demonstrated the broad potential-window of BDD in the degradation and detection of atrazine in chip mode, achieving the lowest LOD reported to date. Another advantage of our microfluidic platform is its use of relatively small reagent volumes, a feature that is critical for miniaturization and versatility and that could be exploited to create automatic control systems for application such as environmental monitoring.

Based on our promising results with this microfluidic platform, we are confident that it could be selectively tuned to detect and degrade various other contaminants. We envision that this type of device should ultimately prove interesting for applications in environmental monitoring and remediation, and in safety and security.

Acknowledgements

The authors acknowledge the support given by MICINN for the projects MAT2011-25870 and Spain-Japan International Bilateral PIB2010JP-00278.

References

Affam, AC., and Chaudhuri, M., 2013, J. Environ. Manage. 130, 160-165.

Ambrosi, A., Guix, M., Merkoçi, A., 2011, Electrophoresis 32 (8), 861-869.

Aragay, G., Pino, F., and Merkoçi, A., 2012, Chem. Rev. 112 (10), 5317-5338.

Aragay, G., Pons, J., and Merkoçi, A., 2011, Chem. Rev. 111 (5), 3433-3458.

Borràs, N., Oliver, R., Arias, C., and Brillas. E., 2010, J. Phys. Chem. A. 114, 6613–6621.

Chen, X., Hu, X., An, L., Zhang, N., Xia, D., Zuo, X., and Wang, X., 2014, Electrocatalysis 5(1), 68-74.

Drechsel, L., Schulz, M., von Stetten, F., Moldovan, C., Zengerle, R., and Paust, N., 2015, Lab Chip 5(3), 704-710.

Einaga, Y., 2010, Appl. Electrochem. 40, 1807-1816.

Fierro, S., Yoshikawa, M., Nagano, O., Yoshimi, K., Saya, H., and Einaga, Y., 2012, Sci. Rep. 2, 1-6.

George, S.E., Chadwick, R.W., Kohan, M.J., Allison, J.C., Warren, S.H., Williams, R.W., 1995, Environ. Mol. Mutagen. 26(2), 178-184.

Grennan, K., Strachan, G., Porter, A. J., Killard, A. J., and Smyth, M. R., 2003, Anal. Chim. Acta. 500, 287-298.

Hernandez, F., Hidalgo, C., Sancho, J. V., and López, F. J., 1998, Anal. Chem. 70, 3322-3328.

Leovac, A., Vasyukova, E., Ivancev-Tumbas, I., Uhl, W., Kragulj, M., Trickovi, J., Kerkeza, Đ., and Dalmacija, B., 2015, RSC Adv. 5, 8122-8133.

Llopis, X., Pumera, M., Alegret, S., and Merkoçi, A., 2009, Lab Chip 9, 213-218.

Madsen, H.T., Søgaard, E. G. and Muff, J., 2014, Chemosphere. 109, 84-91.

Maleki, N., Absalan, G., Safavi, A., Farjami, E., 2007, Anal. Chim. Acta 581, 37-41.

Malpass, G.R.P., Miwa, D.W., Gomes, L., Azevedo, L, EB., Vilela, WFD., Fukunaga, MT., Guimaraes, JR., Bertazzoli, R., Machado, SAS., and Motheo, A.J., 2010, Water Sci Technol. 62(12), 2729-2736.

Marrero Vera, Y., de Carvalho, R. J., Torem, M. L., and Calfa, B. A., 2009, Chem Eng J. 155(3), 691-697.

Marselli, B., Garcia-Gomez, J., Michaud, P.A., Rodrigo, M.A., and Comninellis, Ch., 2003, J. Electrochem. 150, 79-83.

Medina-Sánchez, M., Miserere, S., and Merkoçi. A., 2012, Lab Chip 12, 1932-1943.

Merkoçi, A., and Kutter, J. P., 2012, Lab Chip 12, 1915-1916.

Merkoçi. A., 2010, Biosens. Bioelectron. 26, 1164-1177.

Minghua, Z., Heikki, S., and Mika, S., 2011, Sep Purif Technol. 78 (3), 290–297.

Min-Jung, S., Jong-Hoon, K., Seung-Koo, L., Dae-Soon, L., Sung Woo, H., and Dongmok, W., 2011, Electroanal. 10, 2408-2414.

Oturan, N., Zhou, M., and Oturan, M.A., 2010, J. Phys. Chem. 114 (39), 10605–10611.

Samet, Y., Agengui, L., and Abdelhédi, R., 2010, Chem. Eng. 161, 167–172.

Samet, Y., Agengui, L., and Abdelhédi. R., 2010, J. Electroanal. Chem. 650(1), 152–158.

Suzuki, A., Ivandini, T. A., Yoshimi, K., Fujishima, A., Oyama, G., Nakazato, T., Hattori, N., Kitazawa, S., and Einaga. Y., 2007, Anal. Chem. 79, 8608-8615.

Tang, L. and Lee, N. Yoon., 2010, Lab Chip 10, 1274-1280.

Vera, Y. M., de Carvalho, R. J., Torem, M. L., and Calfa, B. A., 2009, Chem. Eng. 155, 691–697.

Xia, Y., and Whitesides, G. M., 1998, Annu. Rev. 28, 153-184.

Yuan, Y., Zhou, Y., Wu, L., and Zhi, J., 2012, Int. J. Electrochem. 1-10.

Zou, Y., Xiang, C., Sun, L.X., and Xu, F., 2008, Biosens. Bioelectron. 23, 1010-1016.

http://water.epa.gov/drink/contaminants/basicinformation/atrazine.cfm

Schemes captions

Scheme 1. Schematic of the platform for detection and degradation of atrazine, showing the degradation chip, which is based on a bare boron-doped diamond electrode (A); the micro-mixer for the atrazine magneto-EIA inside the chip (B); and the detection chip, which is based on a boron-doped diamond electrode modified with PtNPs (C). The proposed mechanisms of atrazine degradation (A') and detection (C') are also shown. Inset: (1) Desethyl-Atz, (2 Desethyldeisoproppyl-Atz, (3) Cyanuric acid, (4) Atz, (5) OH^-, (6) H_2O, (7) Reduced HRP, (8) Oxidized HRP, (9) Pt-NPs, (10) MBs-αAtz, and (11) H_2O_2.

Figures captions

Figure 1. Characterization of boron-doped diamond (BDD) electrodes. (A) SEM image of the bare BDD electrode (inset at right: zoom); (B) BDD modified with platinum nanoparticles (PtNPs); (C) Typical Raman spectrum of the BDD electrode; and (D) Plot of the size distribution of the PtNPs.

Figure 2. Detection of atrazine using a microfluidic platform based on a magneto-EIA and BDD/PtNPs electrode. (A) Amperometric measurements taken at -250 mV for different concentrations of atrazine (range: 0.0045 nM to 45 nM) vs. the Ag/AgCl reference electrode; (B) Calibration curve (the error bars correspond to the repeatability of measurements taken on the same chip); and (C) Calibration curve for detection of atrazine (the error bars correspond to the reproducibility of measurements taken on three different chips and conjugations).

Figure 3. Complete magneto-EIA for detection of atrazine using a micro-mixer coupled to the BDD/PtNP-based detection platform. (A) Current peaks for different concentrations of atrazine (range: 0.9 nM to 4.5 nM); and (B) the corresponding calibration curve.

Figure 4. Degradation and detection of atrazine. (A) Chronoamperometric response of residual atrazine (initial Atz concentration 30 nM) post-degradation at different current values; and (B) Degradation (anodic oxidation; expressed as percentage) of atrazine plotted against applied current.

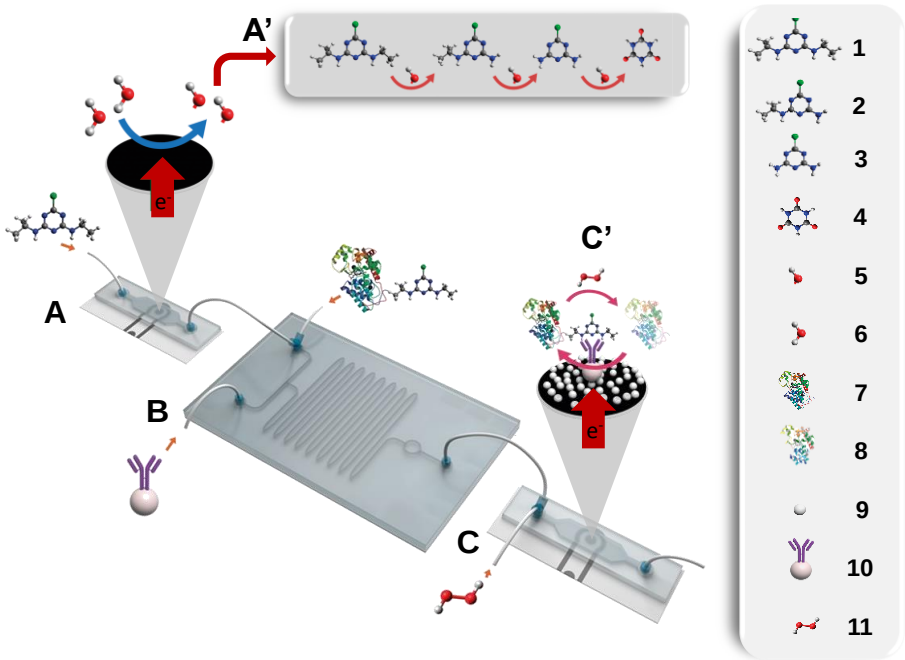

Figure 1.

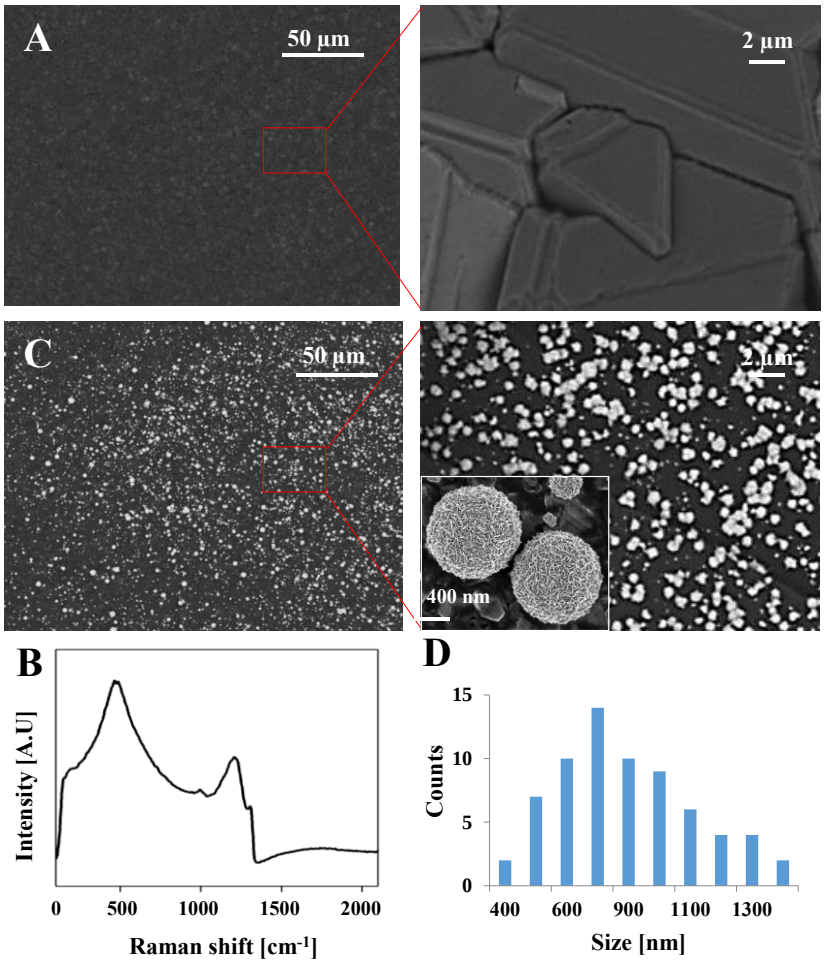
A
50 µm
2 µm
C
50 µm
2 µm
400 nm
B
Intensity [A.U]
0
500
1000
1500
2000
Raman shift [cm-1]
D
Counts
15
10
5
0
400
600
900
1100
1300
Size [nm]

Figure 2.

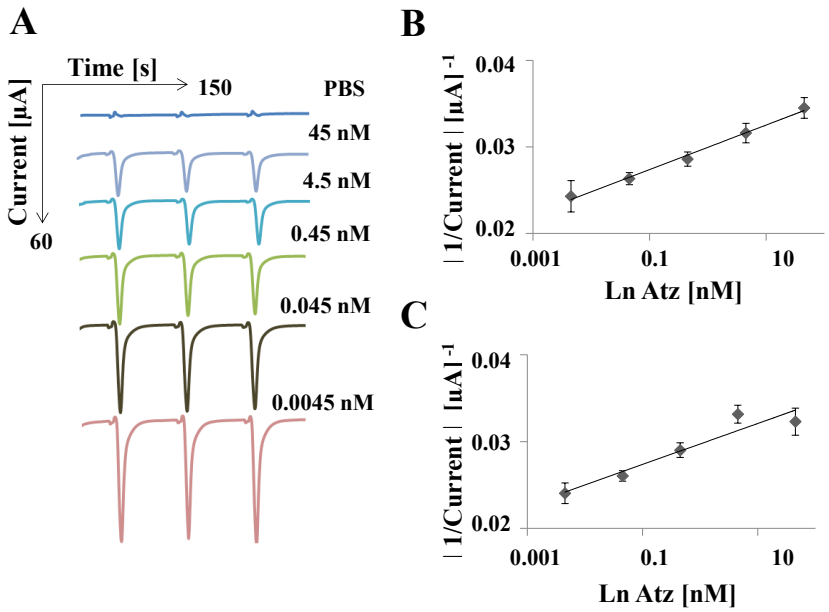
A
Time [s]
150
60
Current [µA]
PBS
45 nM
4.5 nM
0.45 nM
0.045 nM
0.0045 nM
B
| 1/Current | [µA] -1
0.04
0.03
0.02
0.001
0.1
10
Ln Atz [nM]
C
| 1/Current | [uA] -1
0.04
0.03
0.02
0.001
0.1
10
Ln Atz [nM]

Figure 3.

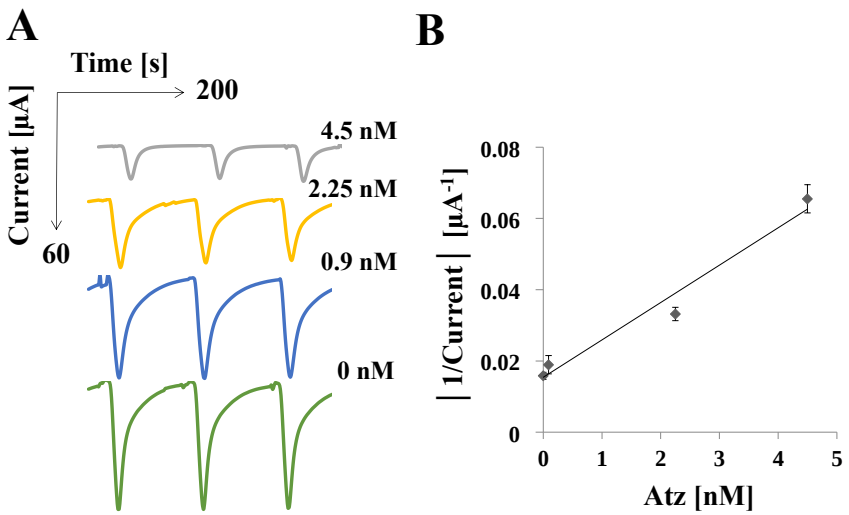
A
Time [s]
200
60
Current [µA]
4.5 nM
2.25 nM
0.9 nM
0 nM
B
0.08
0.06
0.04
0.02
0
0
1
2
3
4
5
| 1/Current | [µA-1]
Atz [nM]

Figure 4.

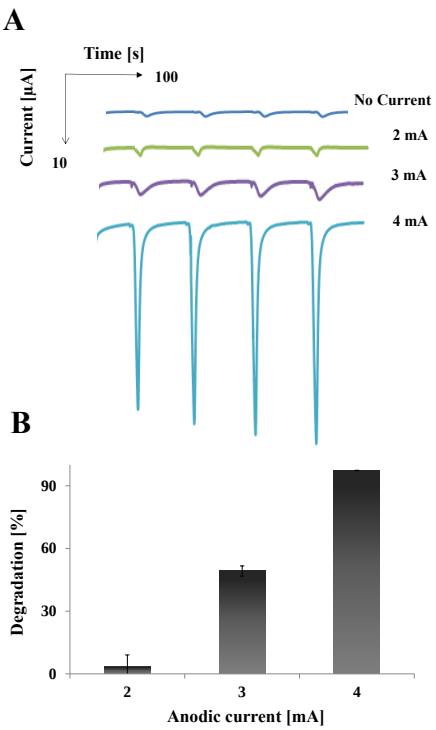
A
Time [s]
100
Current [µA]
10
No Current
2 mA
3 mA
4 mA
B
Degradation [%]
90
60
30
0
2
3
4
Anodic current [mA]

Figure 5.